Continuous and Distribution-free Probabilistic Wind Power Forecasting

Honglin Wen, *Student Member, IEEE,* Pierre Pinson, *Fellow, IEEE,* Jinghuan Ma, Jie Gu, and Zhijian Jin

Abstract—We present a data-driven approach for probabilistic wind power forecasting based on conditional normalizing flow (CNF). In contrast with the existing, this approach is distribution-free (as for non-parametric and quantile-based approaches) and can directly yield continuous probability densities, hence avoiding quantile crossing. It relies on a base distribution and a set of bijective mappings. Both the shape parameters of the base distribution and the bijective mappings are approximated with neural networks. Spline-based conditional normalizing flow is considered owing to its non-affine characteristics. Over the training phase, the model sequentially maps input examples onto samples of base distribution, given the conditional contexts, where parameters are estimated through maximum likelihood. To issue probabilistic forecasts, one eventually maps samples of the base distribution into samples of a desired distribution. Case studies based on open datasets validate the effectiveness of the proposed model, and allows us to discuss its advantages and caveats with respect to the state of the art.

Index Terms—Conditional normalizing flow, deep learning, density estimation, probabilistic forecasting, wind power.

NOMENCLATURE

Functions

$\phi(\cdot)$　　The function that estimates the shape parameters of base distribution

$\tau_k(\cdot)$　　The transformer function in the k-th transform that maps $z_{t,i}^{(k-1)}$ to $z_{t,i}^{(k)}$

$c_k(\cdot)$　　The conditioner function in the k-th transform that outputs the conditionals

$f_{Y_{i,t}}(\cdot)$　Probability density function of $Y_{i,t}$

$q^{(\alpha)}(\cdot)$　Quantile function with level α

$T_k(\cdot)$　　The function that maps $\boldsymbol{z}_t^{(k-1)}$ to $\boldsymbol{z}_t^{(k)}$

Models

$\mathcal{G}$　　　The model for base distribution

$\mathcal{M}$　　　The whole model

Random variables

$\boldsymbol{Y}_t$　　　The random variable for wind power generation values in general form at time t

$\boldsymbol{Z}_t$　　　The intermediate random variable at time t

$Y_{i,t}$　　The random variable for wind power generation value at wind farm i at time t

Variables

$\boldsymbol{x}_t$　　　The input features at time t

$\boldsymbol{y}_t$　　　The realization of $\boldsymbol{Y}_t$

$\boldsymbol{z}_t$　　　The realization of $\boldsymbol{Z}_t$

Honglin Wen, Jinghuan Ma, Jie Gu, and Zhijian Jin are with Department of Electrical Engineering, Shanghai Jiao Tong University.
Honglin Wen, Pierre Pinson are with the Technical University of Denmark, Department of Technology, Management and Economics.

I. INTRODUCTION

A. Motivation

As an essential tool to assess and accommodate wind power generation uncertainty, short-term probabilistic wind power forecasting (PWPF) has gained increasing interest in recent decades. It generally takes numerical weather prediction and historical values as input features, in order to model and communicate the probability density of wind power generation at some time in the future. Such densities may be for a unique lead time and location (hence, univariate), or jointly for several lead times and/or locations (referred to as multivariate) [1]. It has become common now to decouple the estimation of the marginal probability density function of each variable and of the interdependence structure in the multivariate PWPF [2]. In other words, univariate case is usually recognized as the cornerstone of PWPF problems.

A classical approach relies on assumptions (often referred to as parametric approach) for the distribution of future wind power generation, the parameters of which are estimated via statistical and machine learning methods. For instance, the Gaussian, Beta, Generalized Logit-Normal, etc could be used [3]. Although it is convenient to develop models based on such assumptions, the distribution of wind power at hand may not match the assumptions. This is primarily due to the wind power generation process, in other words, the nonlinear power curve that converts energy from the wind into electric power [4]. Concretely, the characteristics of wind power generation distributions differ a lot depending on predicted weather conditions, as illustrated by [5] for instance. This has motivated many to look for distribution-free approaches, i.e., that do not rely on a specific assumption for the densities to model and communicate as forecasts. Certainly the most popular distribution-free approach, also referred to as non-parametric, is quantile regression (QR) [6], which allows to relax the use of distributional assumptions for the case of univariate probabilistic forecasting. It has achieved great success in the Global Energy Forecasting Competition 2014 (GEFCom 2014) for instance, and has become a mainstream solution owing to its state-of-the-art performance and simplicity of use. However, it requires parallel models to be fitted for each quantile, which raises the cost of computation when the whole distribution is needed. In addition, it only provides discrete quantiles, which may lead to quantile crossing – quantiles of the whole distribution are inconsistent.

Till now, parametric models with distributional assumption and QR are still the most effective methods [1] with prominent characteristics. That is, parametric models characterize the whole distribution efficiently, whereas QR models are free of distributional assumptions. For multivariate PWPF, the

complex interdependence structures of multivariate distribution can be modeled using copula models [7]. By estimating the marginal probability density function (PDF) via non-parametric methods and modeling the complex interdependence structure, the copula method is allowed to model complicated multivariate distribution. However, the copula-based approach relies on strong assumptions regarding the probabilistic calibration of predicted marginals, while it often underestimate the strength of the dependence structure among the various variables. Eventually, it remains an open issue to develop an efficient, continuous and distribution-free probabilistic forecasting model that obtains whole distribution at once and is comparable to the state-of-the-art.

B. Related Works

Univariate probabilistic forecasting usually translates to communicating quantile forecasts, prediction interval (PI), and predictive densities. The quantile forecasts and PI are specific characteristics of predictive densities, which are most often obtained by QR. Based on this approach, several machine learning models such as neural network (NN) [8] and gradient boost machine [9] have been adopted to estimate the conditional quantile function. It is then simple and effective to construct PI with two corresponding quantile functions. A $(1-\beta) \times 100\%$ PI can be constructed by the pair of quantiles $(\alpha, 1-\beta+\alpha)$ where $\alpha \in (0, \beta)$, for instance $(\beta/2, 1-\beta/2)$ as typically derived in the literature [10], [11]. However, both PIs and quantiles only provide partial information of probability densities, the applications of which can hardly cover stochastic power system operations where the whole distribution of future wind power generation is often required.

As a result of this, it has been an active research topic to communicate densities in the PWPF community. Besides the aforementioned parametric models, resampling and advanced density estimation techniques have been adopted, as reviewed in [1], [12]. The idea of resampling method lies in estimating the PDF of empirical errors of point forecasts, which makes the method naturally distribution-free. In order to issue conditional densities for the PWPF, fuzzy inference has been applied to classify the forecast conditions into several modes [5]. But such finite classifications cannot continuously adapt to all forecasting conditions. Furthermore, the quality of the estimated densities is strongly related to the performance of utilized point-forecast model. The non-parametric density estimation method, namely kernel density estimation (KDE) has been popular among the PWPF community due to its universal approximation capability. In particular, it generally deduces the density of a finite population selected by k-nearest neighbors [13]. As with the resampling method, this method is still limited in modeling conditional densities, since the employed k-nearest neighbors operation is restricted in dealing with heterogeneous distribution. That said, once k is fixed, the KDE-based model cannot adaptively select the finite population. In addition, the k-nearest neighbor operation suffers from the curse of dimension. Recently, mixture density network (MDN) has been applied in PWPF, as it can model more complex distribution (compared to a Gaussian) through

the comic combination of Gaussian distribution [14]. But it would get stuck in mode collapse issues, which translates to saying that the ultimate distribution would collapse into a Gaussian distribution [15].

Multivariate probabilistic forecasting often communicates *scenarios* as forecasts, which are samples drawn from predictive densities. The scenario generation procedure is based on probability integral transform (PIT) and the interdependence structure characterized by a covariance matrix [2]. Concretely, one draws realizations from the estimated multivariate standard Gaussian distribution, and converts the realizations into scenarios of wind power generation via inverse PIT. Besides, the emerging approach is to directly learn multivariate densities based on advanced generative models such as the generative adversarial network (GAN) adopted in [16]. The GAN is composed of a generator and a discriminator, where the generator is responsible for generating scenarios at the operation stage. Although it is computationally more efficient than the copula method, it suffers from notorious training instability caused by the game between the generator and discriminator at the training phase [17]. Moreover, it only presents the applicability of GAN in generating scenarios, and as such is not focused on producing various forms of probabilistic forecasts e.g. predictive densities in univariate and multivariate setups. Indeed, it has not even been assessed by proper statistical scores. The most related work is [18], which compares the performance of several generative models, i.e., GAN, variational auto-encoder, and an integration-based normalizing flow (NF). But their primary focus is to compare the performance of deep-learning based generative models. It is reported in [18] that the performance of the integration-based NF is limited, let alone compared to state-of-the-art QR models. Besides, they are unaware of the differences between affine NF (which is indeed is equivalent to parametric models with Gaussian distribution assumption) and integration-based NF models. Therefore it leaves issues such as applicability of NF and the relationship between NF with existing models uncovered.

C. Proposed Method and Main Contributions

As a basis for this work, we get inspiration from [5] and [19], which relied on the idea of transforming samples of bounded stochastic process at hand to make them more suitable to be modeled by a Gaussian (or multivariate Gaussian) variable. Besides, parametric models always serve as good candidates for estimating the underlying distributions of wind power generation [20]. Thus, it is appealing to set a parametric model to learn a base distribution, and transform the base distribution to the desired distribution (in the view of the underlying distribution of wind power generation) with an affordable cost. Indeed, it is allowed by the *conservation of probability measure* [21], which translates into saying that one can transform a variable that follows an arbitrary kind of distribution into a variable that follows a desired distribution with the assistance of bijective mapping (transform). Here, instead of using a manually designed transform, we implement such transforms via the NF [22], [23]. An NF
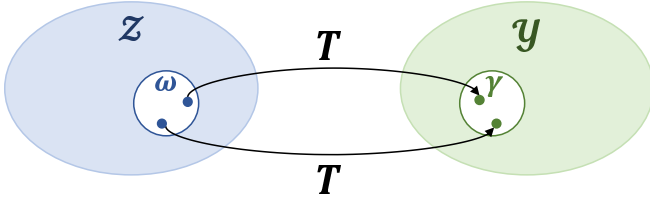
Fig. 1: Illustration of transform.

framework is composed of a base distribution and a sequence of trainable bijective mappings. Both the shape parameters of base distribution and bijective mappings are modeled by neural networks (NNs). Besides, such transforms ought to be non-affine so that the model can flexibly characterize the wind power distribution under different conditions.

Concretely, we establish a distribution-free PWPF model based on a combination of a parametric model with Gaussian distribution assumption and a conditional auto-regressive NF [24], which is applicable to both univariate PWPF and multivariate PWPF applications. Unlike copula models where the marginal PDF and interdependence structure are modeled separately, here the joint probability density is derived through the chain rule of probability, i.e., the product of conditional probability densities. In particular, such conditional probability densities are also dependent on input features. The shape parameters of base Gaussian distribution are learned by the parametric model, whose realizations are then mapped into those of the desired distribution via a spline-based NF [25]. By using the non-affine characteristics of spline-based NF, the model is allowed to characterize the predicted distribution of wind power generation more flexibly. The spline operates in an elementwise manner, i.e., the mapping for each dimension is specified by the outputs of an NN that takes contextual features and the values of previous dimension as inputs. All the parameters are estimated simultaneously based on the maximum likelihood. Case studies validate the effectiveness of the proposed model, which achieves state-of-the-art.

The main contributions of the paper are: (i) The proposal of a distribution-free PWPF model, which suffices to handle the bounded characteristics of wind power by using the power of a parametric model with Gaussian distribution assumption and non-affine transforms. (ii) The demonstration of its applicability to model the whole predictive distribution, which avoids the quantile crossing issue in the univariate PWPF and still presents competitive performance that is comparable to state-of-the-art QR models. (iii) A new perspective for conditional PDF estimation for PWPF based on the function theory, which offers complimentary understanding to merits and caveats of distribution-free approaches versus parametric approaches.

The remainder of this paper is organized as follows. In section II, the problem formulation and methodological components of normalizing flows are introduced. Our approach to their application to univariate and multivariate wind power probabilistic forecasting is described in section III. Section IV summarizes data sources and experiment implementation. The results obtained are presented in Section V, where the performance comparison with existing models is discussed. Section VI concludes this paper.

II. METHODOLOGICAL COMPONENTS

A. Preliminaries

The most important base property to consider for normalizing flows is the concept of conservation of probability measure.

***Definition 1* (Conservation of Probability Measure)** : Denote the PDF defined on $\mathcal{Z} \subseteq \mathbb{R}^d$ as $f_Z(\boldsymbol{z}) : \mathcal{Z} \to [0, +\infty)$, the PDF defined on $\mathcal{Y} \subseteq \mathbb{R}^d$ as $f_Y(\boldsymbol{y}) : \mathcal{Y} \to [0, +\infty)$, and an invertible transform as $T : \mathcal{Z} \to \mathcal{Y}$. For any subset $\omega \subseteq \mathcal{Z}$, we have

$$\int_{\boldsymbol{z} \in \omega} f_Z(\boldsymbol{z})d\boldsymbol{z} = \int_{\boldsymbol{y} \in \gamma} f_Y(\boldsymbol{y})d\boldsymbol{y}. \tag{1}$$

where $\gamma = \{T(\boldsymbol{z}) | \boldsymbol{z} \in \omega\}$, as illustrated in Fig. 1. By utilizing the change of variable, $\boldsymbol{z} = T^{-1}(\boldsymbol{y})$, we convert the formula into

$$\int_{\boldsymbol{y} \in \gamma} f_Z(T^{-1}(\boldsymbol{y})) |\det J_{T^{-1}}(\boldsymbol{y})| d\boldsymbol{y} = \int_{\boldsymbol{y} \in \gamma} f_Y(\boldsymbol{y}) d\boldsymbol{y},$$

where $J_{T^{-1}}(\boldsymbol{y})$ denotes the Jacobian matrix s.t.

$$J_{T^{-1}}(\boldsymbol{y})_{i.j} = \frac{\partial y_i}{\partial z_j}.$$

As it holds for any subset $\gamma \subseteq \mathcal{Y}$, we have

$$f_Y(\boldsymbol{y}) = f_Z(T^{-1}(\boldsymbol{y})) |\det J_{T^{-1}}(\boldsymbol{y})|. \tag{2}$$

B. Problem Formulation

Consider we have p wind farms whose generation is driven by a multivariate stochastic process. For wind farm i, let $y_{i,t}$ denote the generation value at time t, which is a realization of the corresponding random variable $Y_{i,t}$. Then, let $f_{Y_{i,t}}(y)$ and $F_{Y_{i,t}}(y)$ respectively denote the PDF and cumulative distribution function (CDF) of $Y_{i,t}$. The univariate PWPF boils down to estimating the PDF of $Y_{i,t+H}$, i.e., $\hat{f}_{Y_{i,t+H}|t}$, given information $\Omega_{i,t}$ up to t via a model $\mathcal{M}$, i.e.,

$$\hat{f}_{Y_{i,t+H}|t} = f_{Y_{i,t+H}|t}(y|\Omega_{i,t}; \mathcal{M}, \hat{\Theta}), \tag{3}$$

where H is the forecasting horizon, and $\hat{\Theta}$ represents the estimation of real parameters Θ. Certainly, information from nearby wind farms could be used to improve the forecasts, if available [26]. The information may contain previous wind power generation values, i.e., $\{y_{i,t-l}, \cdots, y_{i,t-1}, y_{i,t}\}$, and some exogenous features such as numerical weather predictions (NWPs). Accordingly, one can also obtain the CDF of $Y_{i,t+H}$ by integrating $\hat{f}_{Y_{i,t+H}|t}$, namely $\hat{F}_{Y_{i,t+H}|t}$, the inverse function of which specifies quantiles. For instance, the predicted α-th quantile $\hat{q}_{t+H|t}^{(\alpha)}$ is given by

$$\hat{q}_{t+H|t}^{(\alpha)} = \hat{F}_{Y_{i,t+H}|t}^{-1}(\alpha). \tag{4}$$

A PI with nominal level $(1 - \beta) \times 100\%$ can be formed by two quantiles, $\hat{q}_{t+H|t}^{(\beta/2)}$ and $\hat{q}_{t+H|t}^{(1-\beta/2)}$, i.e.,

$$[\hat{q}_{t+H|t}^{(\beta/2)}, \ \hat{q}_{t+H|t}^{(1-\beta/2)}]. \tag{5}$$

Indeed, multivariate PWPF aims at communicating the joint probability distribution of a collection of future random variables. For instance, the multivariate PWPF may communicate
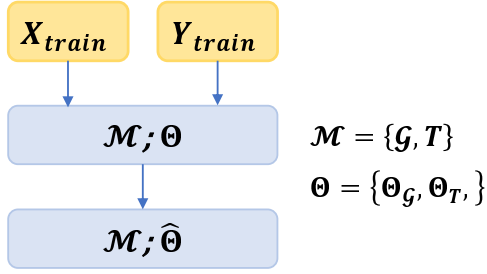
Fig. 2: Illustration of model estimation stage.

Fig. 3: Illustration of operational forecasting stage.

the joint probability distribution of random variables at several future time, i.e., $Y_{i,t+1}, \cdots, Y_{i,t+H}$, which is expressed as

$$\hat{f}_{Y_{i,t+1},\cdots,Y_{i,t+H}|t} = f_{Y_{i,t+1},\cdots,Y_{i,t+H}|t}(\boldsymbol{y}|\Omega_{i,t}; \mathcal{M}, \hat{\Theta}), \quad (6)$$

and that at several sites, i.e.,

$$\begin{aligned} \hat{f}_{Y_{1,t+H},\cdots,Y_{p,t+H}|t} = \\ f_{Y_{1,t+H},\cdots,Y_{p,t+H}|t}(\boldsymbol{y}|\Omega_{1,t},\cdots,\Omega_{p,t}; \mathcal{M}, \hat{\Theta}). \end{aligned} \quad (7)$$

In multivariate PWPF, one often draws several realizations from the distribution as scenarios. For instance, one can draw realizations from $\hat{f}_{Y_{1,t+H},\cdots,Y_{p,t+H}|t}$, which are denoted as $\tilde{y}_{i,t+1}, \cdots, \tilde{y}_{i,t+H}$, i.e.,

$$\tilde{y}_{i,t+1}, \cdots, \tilde{y}_{i,t+H} \sim \hat{f}_{Y_{1,t+H},\cdots,Y_{p,t+H}|t}. \quad (8)$$

Without loss of generality, we write the future random variable as $\boldsymbol{Y}_t$ (which may be univariate or multivariate), and its realization as $\boldsymbol{y}_t$. The information is denoted as Ω_t, whose realization is $\boldsymbol{x}_t$. In this paper, we refer to $\boldsymbol{x}_t$ as contextual features, to make them distinguished from the inputs of NF. Hence, the cornerstone of PWPF can be written in a compact form, i.e.,

$$\hat{f}_{\boldsymbol{Y}_t|t}(\boldsymbol{y}|\boldsymbol{x}_t) = f_{\boldsymbol{Y}_t|t}(\boldsymbol{y}|\boldsymbol{x}_t; \mathcal{M}, \hat{\Theta}). \quad (9)$$

In this paper, we assume that Θ does not change with time, which therefore can be estimated from training datasets $\boldsymbol{X}_{train}$ and $\boldsymbol{Y}_{train}$. It can be also considered in an online setting, where parameters vary with time. With the estimated model at hand, to issue a forecast at time t, it is only required to feed $\boldsymbol{x}_t$ into the model and yield results as described in (9).

The classic parametric approach usually sets $\mathcal{M}$ as a model with distributional assumption, such as Gaussian and Logit-normal, whereas $\hat{\Theta}$ denotes the parameters of a function that maps contextual features to the shape parameters of distribution. With the conservation of probability measure, we consider a intermediate random variable $\boldsymbol{Z}_t$ that follows a specific distribution $f_{\boldsymbol{Z}_t}(\boldsymbol{z})$, whose realization is denoted as $\boldsymbol{z}_t$. Let T map $\boldsymbol{z}_t$ into $\boldsymbol{y}_t$, i.e.,

$$\boldsymbol{y}_t = T(\boldsymbol{z}_t; \hat{\Theta}_T), \quad (10)$$

where $\hat{\Theta}_T$ denotes the estimation of parameters of transform T (whose real parameters are denoted as Θ_T). Now we consider to model the distribution of $\boldsymbol{Z}_t$ via a parametric model $\mathcal{G}$, whose parameters are denoted as $\Theta_{\mathcal{G}}$. The estimation of $\Theta_{\mathcal{G}}$ is denoted as $\hat{\Theta}_{\mathcal{G}}$. Then, the model $\mathcal{M}$ consists of $\mathcal{G}$ and T, i.e., $\mathcal{M} = \{\mathcal{G}, T\}$, whose parameters are $\Theta = \{\Theta_{\mathcal{G}}, \Theta_T\}$. The
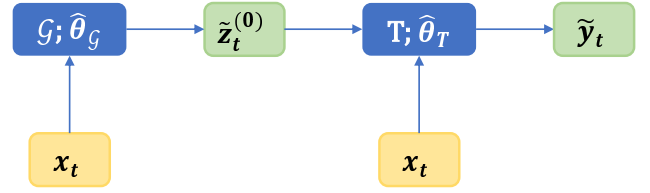
conceptual framework of training stage is shown in Fig. 2. In other words, by learning $\mathcal{G}$ and T, we can estimate the model $\mathcal{M}$.

C. Flow Model for Forecasting

Here we implement the conceptual model T via normalizing flows. Generally, the transform T in an NF consists of a series of invertible functions $T_1, T_2, \ldots, T_K$ [23], i.e.,

$$T = T_1 \circ T_2 \circ \cdots \circ T_K, \quad (11)$$

where $\circ$ denotes the symbol of composition. For each T_k, we denote its input as $\boldsymbol{z}_t^{(k-1)}$, which is the realization of the random variable $\boldsymbol{Z}_t^{(k-1)}$. Accordingly, its output is denoted as $\boldsymbol{z}_t^{(k)}$, which is the realization of the random variable $\boldsymbol{Z}_t^{(k)}$. Particularly, $\boldsymbol{Z}_t^{(0)}$ follows the base distribution specified by $\mathcal{G}$, whereas $\boldsymbol{Z}_t^{(K)}$ is $\boldsymbol{Y}_t$. For simplicity of notations, we drop subscript of density function in what follows.

Two significant calculation passes in NF models are forward and inverse passes. Such computation between $\boldsymbol{z}_t^{(k)}$ and $\boldsymbol{z}_t^{(k-1)}$ for instance is respectively described as

$$\boldsymbol{z}_t^{(k)} = T_k(\boldsymbol{z}_t^{(k-1)}; \hat{\Theta}_{T_k}), \quad \boldsymbol{z}_t^{(k-1)} = T_k^{-1}(\boldsymbol{z}_t^{(k)}; \hat{\Theta}_{T_k}),$$

where $\hat{\Theta}_{T_k}$ represents the estimated parameters of T_k. In particular, we obtain $f(\boldsymbol{z}_t^{(k)}|\boldsymbol{x}_t)$ through $f(\boldsymbol{z}_t^{(k-1)}|\boldsymbol{x}_t)$ and the mapping T_k, which is bijective in $\boldsymbol{z}_t^{(k-1)}$ as well as $\boldsymbol{z}_t^{(k)}$ and parameterized by $\boldsymbol{x}_t$ [27]. We have

$$\begin{aligned} f(\boldsymbol{z}_t^{(k)}|\boldsymbol{x}_t) &= f(\boldsymbol{z}_t^{(k-1)}|\boldsymbol{x}_t)|\frac{\partial \boldsymbol{z}_t^{(k-1)}}{\partial \boldsymbol{z}_t^{(k)}}| \\ &= f(T_k^{-1}(\boldsymbol{z}_t^{(k)}; \hat{\Theta}_{T_k}, \boldsymbol{x}_t)|\boldsymbol{x}_t)|\det J_{T_k}(\boldsymbol{z}_t^{(k-1)})|. \end{aligned} \quad (12)$$

Consequently, the forward and inverse passes in CNF are expressed as

$$\boldsymbol{z}_t^{(k)} = T_k(\boldsymbol{z}_t^{(k-1)}; \hat{\Theta}_{T_k}, \boldsymbol{x}_t), \quad \boldsymbol{z}_t^{(k-1)} = T_k^{-1}(\boldsymbol{z}_t^{(k)}; \hat{\Theta}_{T_k}, \boldsymbol{x}_t). \quad (13)$$

With the sequential transforms, we have

$$\boldsymbol{y}_t = T(\boldsymbol{z}_t^{(0)}; \hat{\Theta}_T, \boldsymbol{x}_t), \quad \boldsymbol{z}_t^{(0)} = T^{-1}(\boldsymbol{y}_t; \hat{\Theta}_T, \boldsymbol{x}_t).$$

where $\hat{\Theta}_T$ denotes the parameters of T, which is a collection of $\hat{\Theta}_{T_k}$, i.e., $\hat{\Theta}_T = \{\hat{\Theta}_{T_1}, \cdots, \hat{\Theta}_{T_K}\}$.

The Jacobian determinant is computed by

$$\begin{aligned} \log|\det J_T(\boldsymbol{z}_t^{(0)})| &= \log|\prod_{k=1}^{K} \det J_{T_k}(\boldsymbol{z}_t^{(k-1)})| \\ &= \sum_{k=1}^{K} \log|\det J_{T_k}(\boldsymbol{z}_t^{(k-1)})|. \end{aligned}$$

Ultimately, we build the connection between the PDF of $z_t^{(0)}$ and that of y_t, i.e.,

$$\log f(\boldsymbol{y}_t) = \log f(\boldsymbol{z}_t^{(0)}) + \sum_{k=1}^{K} \log |\det J_{T_k}(\boldsymbol{z}_t^{(k-1)})|.$$

Such T_k in the NF model is implemented via NNs, and is required to be invertible and have a tractable Jacobian determinant.

The introduced CNF model is trained based on maximum likelihood. As we assume that parameters Θ will not change with time, we can estimate them from training dataset $\boldsymbol{Y}_{train} = [\boldsymbol{y}_1, \boldsymbol{y}_2, \cdots, \boldsymbol{y}_N]^\top$ and $\boldsymbol{X}_{train} = [\boldsymbol{x}_1, \boldsymbol{x}_2, \cdots, \boldsymbol{x}_N]^\top$. The loss function is defined as

$$\mathcal{L} = -\frac{1}{N} \sum_{n=1}^{N} \log f(\boldsymbol{y}_n | \boldsymbol{x}_n)$$
$$= -\frac{1}{N} \sum_{n=1}^{N} [\log f(T^{-1}(\boldsymbol{y}_n, \boldsymbol{x}_n)) + \log |\det J_T(T^{-1}(\boldsymbol{y}_n, \boldsymbol{x}_n))|].$$
$$(14)$$

At the training stage, we estimate $\hat{\Theta}$ by minimizing loss function $\mathcal{L}$. To issue forecasts at time t, we feed $\boldsymbol{x}_t$ into the base model and all transforms, which is illustrated in Fig. 3. Then, we derive the density of $\boldsymbol{z}_t^{(0)}$, i.e.,

$$\hat{f}(\boldsymbol{z}_t^{(0)} | \boldsymbol{x}_t; \mathcal{G}, \hat{\Theta}_{\mathcal{G}}).$$

Based on it, we could draw L realizations:

$$\tilde{\boldsymbol{z}}_t^{(0),1}, \cdots, \tilde{\boldsymbol{z}}_t^{(0),L} \sim \hat{f}(\boldsymbol{z}_t^{(0)} | \boldsymbol{x}_t; \mathcal{G}, \hat{\Theta}_{\mathcal{G}}). \quad (15)$$

By transforming each realization $\tilde{\boldsymbol{z}}_t^{(0),i}$ via T, i.e.,

$$\tilde{\boldsymbol{y}}_t^i = T(\tilde{\boldsymbol{z}}_t^{(0),i}; \boldsymbol{x}_t, \hat{\Theta}_T), \quad (16)$$

we can obtain L realizations of $\hat{f}(\boldsymbol{y}_t | \boldsymbol{x}_t; \mathcal{M}, \hat{\Theta})$, namely $\tilde{\boldsymbol{y}}_t^1, \cdots, \tilde{\boldsymbol{y}}_t^L$. In particular, we can obtain the α-th quantile of $\hat{f}(\boldsymbol{z}_t^{(0)} | \boldsymbol{x}_t; \mathcal{G}, \hat{\Theta}_{\mathcal{G}})$, which is denoted as $\hat{q}_{\mathcal{G}}^{(\alpha)}$, and then transform it via T to obtain the quantile of $\hat{f}(\boldsymbol{y}_t | \boldsymbol{x}_t; \mathcal{M}, \hat{\Theta})$, i.e.,

$$\hat{q}_{\mathcal{M}}^{(\alpha)} = T(\hat{q}_{\mathcal{G}}^{(\alpha)}; \boldsymbol{x}_t, \hat{\Theta}_T) \quad (17)$$

D. Relationship with Classic Methods

Here we discuss the relationship between this method with classic methods. In what follows, we assume the base distribution as normal distribution, i.e., $\boldsymbol{z}_t^{(0)} \sim \mathcal{N}(\boldsymbol{0}, \boldsymbol{I})$.

1) Gaussian Distribution: Models with the Gaussian distributional assumption [28], [29] can be translated into setting the transform of NF models as an affine transform. That is,

$$\boldsymbol{y}_t = T(\boldsymbol{z}_t^{(0)}) = \boldsymbol{A}_t \boldsymbol{z}_t^{(0)} + \boldsymbol{b}_t,$$

where $\boldsymbol{A}_t$ and $\boldsymbol{b}_t$ are the corresponding matrix and vector specified by $\boldsymbol{x}_t$. Then the problem boils down to estimating $\boldsymbol{A}_t$ and $\boldsymbol{b}_t$ from data. However, as affine transforms cannot change the family of distribution, $\boldsymbol{y}_t$ still obeys Gaussian distribution, i.e.,

$$\boldsymbol{y}_t \sim \mathcal{N}(\boldsymbol{\mu}_t, \Sigma_t),$$

where $\boldsymbol{\mu}_t$ and Σ_t are the corresponding shape parameters. Classic methods usually directly estimate $\boldsymbol{\mu}_t$ and Σ_t via statistical learning, instead of $\boldsymbol{A}_t$ and $\boldsymbol{b}_t$.

2) Logit-Normal Distribution: Let $y_{t,i}$ and $z_{t,i}^{(k)}$ respectively represent the i-th element of $\boldsymbol{y}_t$ and $\boldsymbol{z}_t^{(k)}$. Besides, $y_{t,i}$ is normalized into the interval $[0, 1]$. The logit-normal distribution [19] can be interpreted as setting the transform T as a combination of affine transforms and a sigmoid transform. Using the affine transforms, we derive

$$\boldsymbol{z}_t^{(K-1)} \sim \mathcal{N}(\boldsymbol{\mu}_t, \Sigma_t),$$

where $\boldsymbol{\mu}_t$ and Σ_t are specified by $\boldsymbol{x}_t$. Then the logit-normal transform operates element-wise on $\boldsymbol{z}_t^{(K-1)}$, i.e.,

$$y_{t,i} = \frac{\exp(z_{t,i}^{(K-1)})}{1 + \exp(z_{t,i}^{(K-1)})}.$$

3) Mixture Density Network: The model based on mixture density network [14] can be considered as setting T as the conic combination of affine transforms. That is, each component transform T_i operates as

$$T_i(\boldsymbol{z}_t^{(0)}) = \boldsymbol{A}_t^i \boldsymbol{z}_t^{(0)} + \boldsymbol{b}_t^i,$$

where $\boldsymbol{A}_t^i$ and $\boldsymbol{b}_t^i$ are parameters, specified by $\boldsymbol{x}_t$. The transform defined by this model operates as

$$\boldsymbol{y}_t = T(\boldsymbol{z}_t^{(0)}) = \sum_i \omega_i T_i(\boldsymbol{z}_t^{(0)}),$$

where ω_i represents the weight of T_i.

4) Gaussian Copula: The model based on Gaussian Copula [2] is an instance of NF, which is specified by an element-wise monotone function g and a correlation matrix Σ_t specified by $\boldsymbol{x}_t$. That is,
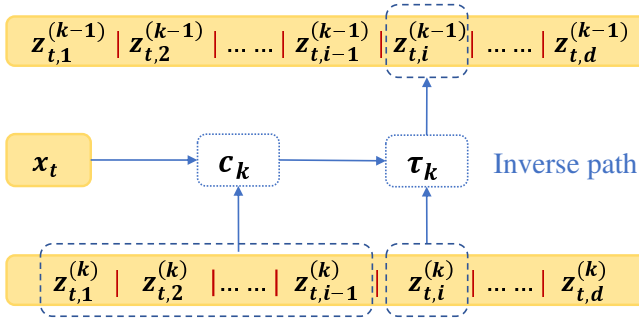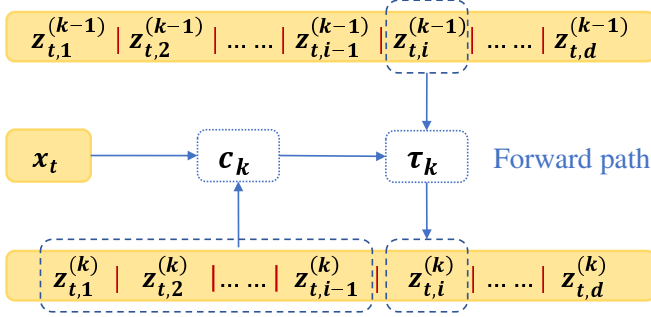
$$\boldsymbol{z}_t^{(K-1)} = \boldsymbol{A}_t \boldsymbol{z}_t^{(0)} \sim \mathcal{N}(\boldsymbol{0}, \Sigma_t),$$

$$y_{t,i} = g(z_{t,i}^{(K-1)}).$$

Indeed, any desired distribution can be obtained by transforming a Gaussian distribution through a specific mapping. Such mapping proceeds each value in the domain in the same manner, such as the aforementioned Logit-Normal transform. It implies that characteristics of the derived wind power distributions remain the same for different wind conditions. Although the conic combination enables deriving more complex distributions compared to Gaussian distributions, it still handles each condition indifferently. With regard to the Gaussian copula model, it is developed for multivariate modeling. By modeling the well-calibrated marginal PDF and correlation structure, one can yield the the ultimate joint probability density in a distribution-free way. However, as mentioned above, it highly relies on the estimation of marginals and tends to underestimate the covariance structure, which often impedes its performance.

III. FORECASTING APPLICATIONS

The basic approach for conditional normalizing flows described in the above can readily be used for forecasting applications, in both univariate and multivariate settings. We choose the Gaussian distribution as base distribution whose

Fig. 4: Illustration of inverse path in the k-th transform.

Fig. 5: Illustration of forward path in the k-th transform.

shape parameters are learned by an NN and adopt a non-affine flow to obtain a piece-wise non-Gaussian distribution. Let $\hat{\boldsymbol{\mu}}_t, \hat{\Sigma}_t$ denote the estimated shape parameters of base distribution, which are determined by a function of $\boldsymbol{x}_t$, namely $\phi(\boldsymbol{x}_t; \hat{\Theta}_{\mathcal{G}})$. In other words, with the Gaussian distributional assumption, the model $\mathcal{G}$ described in Section II-B reduces to the function $\phi(\boldsymbol{x}_t; \hat{\Theta}_{\mathcal{G}})$. It is described as

$$\hat{\boldsymbol{\mu}}_t, \hat{\Sigma}_t = \phi(\boldsymbol{x}_t; \hat{\Theta}_{\mathcal{G}}). \tag{18}$$

A. Probabilistic Forecasting Applications

1) Univariate Probabilistic Forecasting: In the univariate case, each intermediary variable and shape parameters of the Gaussian distribution are scalars, which are rewritten as $z_t^{(k)}$, μ_t, and σ_t. The estimated shape parameters of base distribution $\hat{\mu}_t, \hat{\sigma}_t$ are derived via

$$\hat{\mu}_t, \hat{\sigma}_t = \phi(\boldsymbol{x}_t; \hat{\Theta}_{\mathcal{G}}). \tag{19}$$

T_k is a univariate function that operates as

$$z_t^{(k)} = T_k(z_t^{(k-1)}; \boldsymbol{x}_t, \hat{\Theta}_T). \tag{20}$$

2) Multivariate Probabilistic Forecasting: The most relevant computation to consider for multivariate forecasting is the transform described in (13). Here, let us consider a function τ_k in the transform T_k that operates elementwise and relies on previous dimensions and contextual information. Take the computation of i-th dimension as an example, i.e., the forward path and inverse path between $z_{t,i}^{(k-1)}$ and $z_{t,i}^{(k)}$. In the inverse path, τ_k^{-1} maps $z_{t,i}^{(k)}$ into $z_{t,i}^{(k-1)}$ via

$$z_{t,i}^{(k-1)} = \tau_k^{-1}(z_{t,i}^{(k)}; c_k(\boldsymbol{z}_{t,1:i-1}^{(k)}, \boldsymbol{x}_t; \hat{\theta}_{c_k}), \hat{\theta}_{\tau_k}), \tag{21}$$

where $\boldsymbol{z}_{t,1:i-1}^{(k)}$ represents $[z_{t,1}^{(k)}, \cdots, z_{t,i-1}^{(k)}]^{\top}$, $\hat{\theta}_{\tau_k}$ represents the parameters of τ_k, and $c(\boldsymbol{z}_{t,1:i-1}^{(k)}, \boldsymbol{x}_t; \hat{\theta}_{c_k})$ is a function that outputs conditionals. In other words, $\hat{\Theta}_{T_k}$ contains $\hat{\theta}_{\tau_k}$ and $\hat{\theta}_{c_k}$. The forward path is described as

$$z_{t,i}^{(k)} = \tau_k(z_{t,i}^{(k-1)}; c_k(\boldsymbol{z}_{t,1:i-1}^{(k)}, \boldsymbol{x}_t; \hat{\theta}_{c_k}), \hat{\theta}_{\tau_k}). \tag{22}$$

Using the terminology of [30], $c_k(\cdot)$ and $\tau_k(\cdot)$ are respectively referred to as the conditioner and transformer. Illustration of such calculation procedure is shown in Fig. 4 and Fig. 5.

Remark 1: With the chain rule of probability, we decompose the joint probability density $f(\boldsymbol{z}_t^{(k)} | \boldsymbol{x}_t)$ into a product of conditional probability densities, i.e.,

$$f(\boldsymbol{z}_t^{(k)} | \boldsymbol{x}_t) = \prod_{i=1}^{d} f(z_{t,i}^{(k)} | \boldsymbol{z}_{t,1:i-1}^{(k)}, \boldsymbol{x}_t).$$

As shown in Section II-C, the training stage is relied on the inverse path and the computation of likelihood. Indeed, the inverse path described in (21) is associated with $f(z_{t,i}^{(k)} | \boldsymbol{z}_{t,1:i-1}^{(k)}, \boldsymbol{x}_t)$, which translates into saying that the computation of likelihood will preserve the conditional structure of multivariate distribution. The forward path can be translated into sampling $\boldsymbol{z}_t^{(k-1)}$ from $f(\boldsymbol{z}_t^{(k-1)} | \boldsymbol{x}_t)$ and computing via (22), which can be also regarded as sampling $z_{t,i}^{(k)}$ from $f(z_{t,i}^{(k)} | \boldsymbol{z}_{t,1:i-1}^{(k)}, \boldsymbol{x}_t)$.

Remark 2: The univariate probabilistic forecasting can be interpreted as a special case of multivariate probabilistic forecasting. As with (22), we rewrite (20) as

$$z_t^{(k)} = \tau_k(z_t^{(k-1)}; c_k(\boldsymbol{x}_t; \hat{\theta}_{c_k}), \hat{\theta}_{\tau_k}).$$

B. Base Distribution

The function $\phi(\cdot)$ described in (18) and (19) is implemented by an NN of N_ϕ layers. Denote the outputs, weights, and bias of the l-th layer respectively as $\boldsymbol{h}_t^{\phi,l}$, $\boldsymbol{W}^{\phi,l}$, and $\boldsymbol{b}^{\phi,l}$. The l-th layer operates as

$$\boldsymbol{h}_t^{\phi,l} = \boldsymbol{W}^{\phi,l} \boldsymbol{h}_t^{\phi,l-1} + \boldsymbol{b}^{\phi,l}. \tag{23}$$

Specially, $\boldsymbol{h}_t^{\phi,0} = \boldsymbol{x}_t$. After each layer, a non-linear element-wise operator ReLu$(\cdot)$ is followed, i.e.

$$\text{ReLu}(h_{t,i}^{\phi,l}) = \max(h_{t,i}^{\phi,l}, 0). \tag{24}$$

The output layer will yield $\hat{\boldsymbol{\mu}}_t$ and $\hat{\Sigma}_t$.

C. Non-affine Transform

In this section, we describe the conditioner and transformer of the adopted transform.

1) Conditioner: The function $c_k(\cdot)$ is set as an addictive model and implemented by an NN. Concretely, it contains two parts: the function of $\boldsymbol{z}_{t,1:i-1}^{(k)}$ and the function of $\boldsymbol{x}_t$. Then, $c_k(\cdot)$ is described as

$$c_k(\boldsymbol{z}_{t,1:i-1}^{(k)}, \boldsymbol{x}_t; \hat{\theta}_{c_k}) = c_{k,1}(\boldsymbol{z}_{t,1:i-1}^{(k)}) + c_{k,2}(\boldsymbol{x}_t), \tag{25}$$

where $c_{k,1}(\cdot)$ and $c_{k,2}(\cdot)$ are the two component functions. $c_{k,2}(\cdot)$ is implemented by an NN, similar to that of $\phi(\cdot)$. Specially, as the length of $\boldsymbol{z}_{t,1:i-1}^{(k)}$ changes for each dimension, it is implemented via a model named as MADE [31].

TABLE I: Case study settings.

	Type of variable	Input feature	Forecasting horizon	Type of interdependence	Dataset
Case 1	univariate	NWP	24	none	GEFCom 2014
Case 2	univariate	previous values of length 6	1	none	NREL, France wind farm
Case 3	multivariate	previous values of length 6	6	temporal interdependence	France wind farm
Case 4	multivariate	previous values of length 6	1	spatial interdependence	NREL

TABLE II: Dataset description.

Dataset	Description	Resolution	Samples
GEFCom 2014	NWP that contains wind speed and direction at two altitudes respectively, as well as corresponding wind power values	1-h	16800
France wind farm	Time series of wind power	10-min	52355
NREL	Time series of wind power	15-min	35040

2) Transformer: The main idea of spline-based NF is to implement the transform as monotonic spline [25]. Each τ_k is represented as a piece-wise function which contains M segments specified by $M + 1$ coordinates (knots). The knots are obtained from the conditioner $c_k(\cdot)$ and denoted as $\{(\alpha_{k,m}, \beta_{k,m})|m = 0, \cdots, M\}$. Accordingly, the transformer $\tau_k(\cdot)$ is split into M segments, each of which is a simple monotonic function. Every two nearby segments will meet at internal knots $\{(\alpha_{k,m}, \beta_{k,m})|m = 1, \cdots, M - 1\}$. Specifically, we use monotonic rational-quadratic splines, which are defined by derivatives at internal knots besides the knots. They are also derived from the conditioner $c_k(\cdot)$ and denoted as $\{\delta_{k,m}|m = 1, \cdots, M - 1\}$. We define

$$s_{k,m} = \frac{\beta_{k,m} - \beta_{k,m-1}}{\alpha_{k,m} - \alpha_{k,m-1}},$$

$$\xi(z_{t,i}^{(k-1)}) = \frac{z_{t,i}^{(k-1)} - \alpha_{k,m-1}}{\alpha_{k,m} - \alpha_{k,m-1}}.$$

The rational-quadratic function in the m-th bin is expressed as

$$r_{k,m}(\xi) = \beta_{k,m-1} + \frac{(\beta_{k,m} - \beta_{k,m-1})[s_{k,m}\xi^2 + \delta_{k,m-1}\xi(1-\xi)]}{s_{k,m} + [\delta_{k,m} + \delta_{k,m-1} - 2s_{k,m}]\xi(1-\xi)},$$

where ξ represents $\xi(z_{t,i}^{(k-1)})$. That is,

$$\tau_k(z_{t,i}^{(k-1)}) = r_{k,m}(\xi), \text{ if } z_{t,i}^{(k-1)} \in [\alpha_{k,m-1}, \alpha_{k,m}]. \quad (26)$$

Specifically, when $z_{t,i}^{(k-1)} < \alpha_{k,0}$ or $z_{t,i}^{(k-1)} > \alpha_{k,M}$, we set $\tau_k(\cdot)$ as equivalent transform, i.e.,

$$\tau_k(z_{t,i}^{(k-1)}) = z_{t,i}^{(k-1)}, \text{ if } z_{t,i}^{(k-1)} \in (-\infty, \alpha_{k,0}] \cup [\alpha_{k,M}, \infty). \quad (27)$$

As $\tau_k(\cdot)$ is monotonic, the inverse path can be computed analytically by solving a quadratic equation, i.e.,

$$\xi(z_{t,i}^{(k-1)}) = \frac{2C}{-B - \sqrt{B^2 - 4AC}}, \quad (28)$$

where

$$A = (\beta_{k,m} - \beta_{k,m-1})(s_{k,m} - \delta_{k,m-1}) + (z_{t,i}^{(k)} - \beta_{k,m-1})(\delta_{k,m} + \delta_{k,m-1} - 2s_{k,m}),$$

$$B = (\beta_{k,m} - \beta_{k,m-1})\delta_{k,m-1} - (z_{t,i}^{(k)} - \beta_{k,m-1})(\delta_{k,m} + \delta_{k,m-1} - 2s_{k,m}),$$

$$C = -s_{k,m}(z_{t,i}^{(k)} - \beta_{k,m-1}).$$

It implicitly defines the inverse function $\tau_k^{-1}(\cdot)$.

IV. CASE STUDY

In this paper, we validate the proposed approach in both univariate cases (Case 1, Case 2) and multivariate cases (Case 3, Case 4). Their settings are described as follows and summarized in Table I.

1) Case 1: It is a day-ahead PWPF case based on the GEFCom 2014 data[1], where numerical weather predictions (NWPs) are taken as inputs and predictive PDF of wind power at each time step is issued as forecast.
2) Case 2: It is a very-short-term PWPF case where previous values of wind power generation are taken as inputs, and predictive PDF of wind power at future time is issued as forecast. Horizon is set as 1 here for validation based on the NREL[2] and France wind farm data[3].
3) Case 3: It is a scenario generation case based on the France wind farm data, which considers temporal interdependence. Specifically, we generate scenarios of future 6 time steps, which can be used in electricity market.
4) Case 4: It is a scenario generation case based on the NREL data, which considers spatial interdependence of multiple sites. Horizon is set as 1. Specifically, we choose data from 5 nearby wind farms for validation.

As feature selection is not the focus of this paper, in Case 2, Case 3, and Case 4, the length of input features is determined by a preliminary test, which is varied from 4 to 24 and empirically set as 6. Certainly, models may be further improved by finely selecting the features. But it is fair for all models as they use the same input features.

---

[1] Available at http://blog.drhongtao.com/2017/03/gefcom2014-load-forecasting-data.html

[2] Available at https://www.nrel.gov/grid/wind-toolkit.html

[3] Available at https://opendata-renewables.engie.com/explore/index

A. Dataset Description

Three open datasets are used for validation, i.e., data from GEFCom 2014, NREL, and France wind farm. The GEFCom 2014 dataset provides NWPs that contain wind speeds and directions at 10-m and 100-m, and corresponding normalized wind power generation values. It is an hourly data set collected in 2012 and 2013, and contains a total of 16,800 samples. We randomly select data from 5 wind farms for experiments. The France wind farm data and the NREL data are time series. Data from the France wind farm are collected from four wind turbines, whereas NREL data are generated by simulation at various sites. The resolution of the France wind farm data is 10-min, whereas that of the NREL data is 15-min. Specifically, we select France wind farm data collected in 2013 which contain 52355 samples, and NREL data collected in 2012 which contain 35040 samples for validation. In each case, we split 70% of the data as a training set, 10% as a validation set, and 20% as a test set according to [32]. The information about datasets is summarized in Table II.

B. Assessment Metrics

In this paper, reliability diagrams and PI width are used to assess the reliability and sharpness of univariate predictive densities. The comprehensive quality of predictive probability density in univariate cases is assessed by continuous ranked probability score (CRPS) as suggested by [33]. And the quality of predictive probability density in multivariate cases is assessed by scenarios in terms of energy score (ES) and variogram score (VS) as suggested by [34], [35]. All of them are averaged over the whole test data.

1) CRPS: Let $F_t(y)$ denote the CDF of Y_t and y_t denote the observation at time t. The CRPS is defined as:

$$\mathrm{CRPS}(F_t, y_t) = \int_y (F_t(y) - \mathbb{1}(y - y_t))^2 dy, \quad (29)$$

where $\mathbb{1}(\cdot)$ is unit step function, which represents the empirical CDF of observation.

2) ES: Given a set of scenarios $\{\tilde{\boldsymbol{y}}_t^{(i)} | i = 1, \cdots, S\}$ and observations $\boldsymbol{y}_t$, the ES is defined as

$$\mathrm{ES} = \frac{1}{S} \sum_{i=1}^{S} \|\boldsymbol{y}_t - \tilde{\boldsymbol{y}}_t^{(i)}\|_2 - \frac{1}{2S^2} \sum_{i=1}^{S} \sum_{j=1}^{S} \|\tilde{\boldsymbol{y}}_t^{(i)} - \tilde{\boldsymbol{y}}_t^{(j)}\|_2, \quad (30)$$

where $\| \cdot \|_2$ is the d-dimensional Euclidean norm.

3) VS: Let $y_{t,i}$ and $\tilde{y}_{t,i}$ respectively denote the i-th dimension of the observation $\boldsymbol{y}_t$ and a scenario $\tilde{\boldsymbol{y}}_t$. The VS is defined as

$$\mathrm{VS} = \sum_{i,j=1}^{d} (|y_{t,i} - y_{t,j}|^p - \mathbb{E}(|\tilde{y}_{t,i} - \tilde{y}_{t,j}|^p))^2, \quad (31)$$

where

$$\mathbb{E}(|\tilde{y}_{t,i} - \tilde{y}_{t,j}|^p) \approx \frac{1}{S} \sum_{s=1}^{S} |\tilde{y}_{t,i}^{(s)} - \tilde{y}_{t,j}^{(s)}|^p.$$

Here we set p as 0.5 as suggested by [35].

C. Benchmarks

1) Univariate Cases: We set both parametric models and non-parametric models as benchmarks. For the parametric approaches, we choose NN models that rely on assumptions of Gaussian and logit-normal distributions, and refer to them as NN-G and NN-L respectively. They share the same basic NN structure with the proposed model. An MDN is established, as it is allowed to model more complicated distributions compared to Gaussian distribution. As for the non-parametric approaches, we include two popular distribution-free models KDE [13] and quantile regression gradient boosting machine (QRGBM) [9] as benchmarks since they are proved effective in the GEFCom 2014. The QRGBM is an ensemble model that iteratively fits new tree model to minimize the quantile loss. Concretely, in the KDE, we determine the nearest 100 neighbors of each test sample and use their corresponding wind power values to estimate the predictive PDF. In addition, the climatology model is adopted as a naive benchmark model, which estimates the predictive probability density using all training data.

2) Multivariate Cases: For multivariate cases, we mainly use NN-G, and NN-L as benchmark models, since they are the most popular ones. Besides, multivariate probabilistic ensemble (MuPEn) [36] is adopted as a naive benchmark. It is a generalized model of the complete-history persistence, which conducts random sampling without replacement from historical scenarios for each test data.

D. Implementation Details

1) Univariate Cases: The base distributions of NN-G, NN-L, and the proposed model are set as Gaussian distribution. We carry out preliminary tests to determine the hyperparameters of the proposed model. The NN that determines shape parameters of the Gaussian distributions contains 2 hidden fully connected layers (each has 512 units). For fairness, we use the same amount of transforms (concretely, 5 transforms here) for NN-G, NN-L, and the proposed model. All the transforms are implemented by NNs with 2 hidden fully connected layers, each of which contains 256 units. Such transforms in the proposed model are specified as neural spline transforms[4], whereas they are are designed as affine transforms in the NN-G and NN-L. particularly, for NN-L, we use a sigmoid transform behind the 5 affine transforms. The MDN for use contains 5 Gaussian components, both the weights and shape parameters of which are estimated by an NN.

2) Multivariate Cases: For multivariate cases, NN-G, NN-L and the proposed model use the same NN architecture used for univariate cases. The only difference is that we adopt the auto-regressive structure here to model the joint probability density. It is implemented based on masked auto-encoder [31] that forces each variable to only rely on the previous variables in a given order via masks. Besides, we permute variable orders after each transform, as PDF is permutation-invariant.

NN-G, NN-L, and the proposed model are established via Pytorch and trained by the Adam optimizer [37]. The learning

---

[4]Code will be released upon publication.

TABLE III: CRPS on GEFCom 2014 (percentage of nominal capacity).

	1	3	5	7	9
Climatology	19.30	18.38	21.36	18.10	18.79
NN-G	9.45	8.98	8.51	7.43	8.48
NN-L	9.33	8.62	8.88	7.40	8.88
QRGBM	9.72	8.57	8.32	7.62	8.27
KDE	10.07	8.76	8.64	7.76	8.56
MDN	9.98	8.77	8.32	7.28	9.37
Proposed model	9.08	8.35	8.14	7.09	8.28

Fig. 6: Illustration of probability density of 100-th sample in test set.

rate is determined through a grid search and ultimately set as 1e-4. It decays 1/3 per 300 epochs. The QRGBM is implemented based on lightGBM[5], the hyperparameters of which are set according to the winner of GEFCom 2014 [9]. KDE is implemented by using scikit-learn[6].

V. RESULTS AND DISCUSSION

A. Case 1

1) CRPS: Values of CRPS are presented in Table III. It is seen that all the benchmark models and the proposed model outperform climatology model. Amongst the benchmark models, KDE has slightly lower performance than others, which suggests that it is overly simplified to approximate the conditional PDF by the density of neighborhood population. Concretely, the distribution of samples is not homogeneous, which means more samples could be taken to better estimate the conditional PDF if the neighborhood distribution is dense. However, once the criterion to select neighborhood samples is fixed, e.g. value of k in k-nearest neighbors here, it cannot adaptively adjust the population, on which the conditional PDF estimation is based. On the contrary, NN-G, NN-L, QRGBM, MDN, and the proposed model can adaptively estimate the conditional PDF/quantile by excavating the similarity

[5]https://lightgbm.readthedocs.io/en/latest/
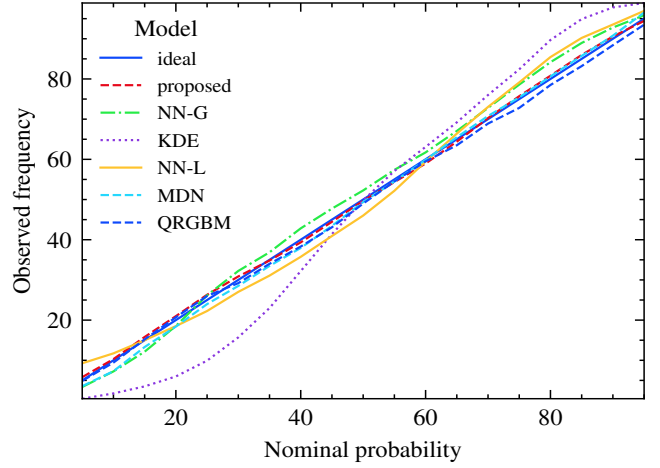[6]https://scikit-learn.org/stable/

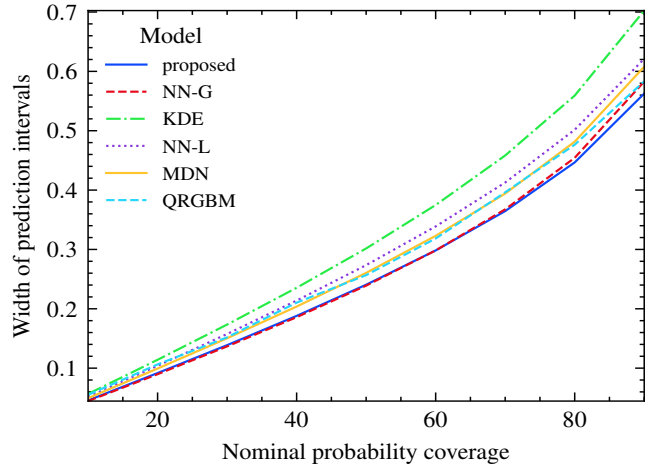Fig. 7: Reliability diagram of forecasts at wind farm 1.

Fig. 8: Width of PI at wind farm 1.

of input features via parameterization or entropy measure. It also suggests that the performance of KDE can be further improved by carefully designing such population selection criterion and making use of the similarity of neighborhood samples. The QRGBM outperforms the NN-G and NN-L in 3/5 of cases as it is distribution-free. However, the other two cases suggest that the independent fitting in QRGBM may accumulate errors. MDN is comparable with NN-G and NN-L, which may be explained as that it is harder to estimate weights and component distributions jointly in the MDN compared to NN-G and NN-L (where only shape parameters are required to be estimated). Furthermore, once the weights are fixed, they cannot specifically adapt to each wind condition. Obviously, the proposed model exceeds benchmarks in all cases.

The comparison between NN-L and NN-G shows that logit-normal transform may degenerate performance at times. It reveals that the logit-normal distribution assumption may not match the real distribution sometimes, although the variable is forced to fall into the physical constraints. We present the predictive probability density of the proposed model at a selected timestamps in Fig. 6. As illustrated, the PDF
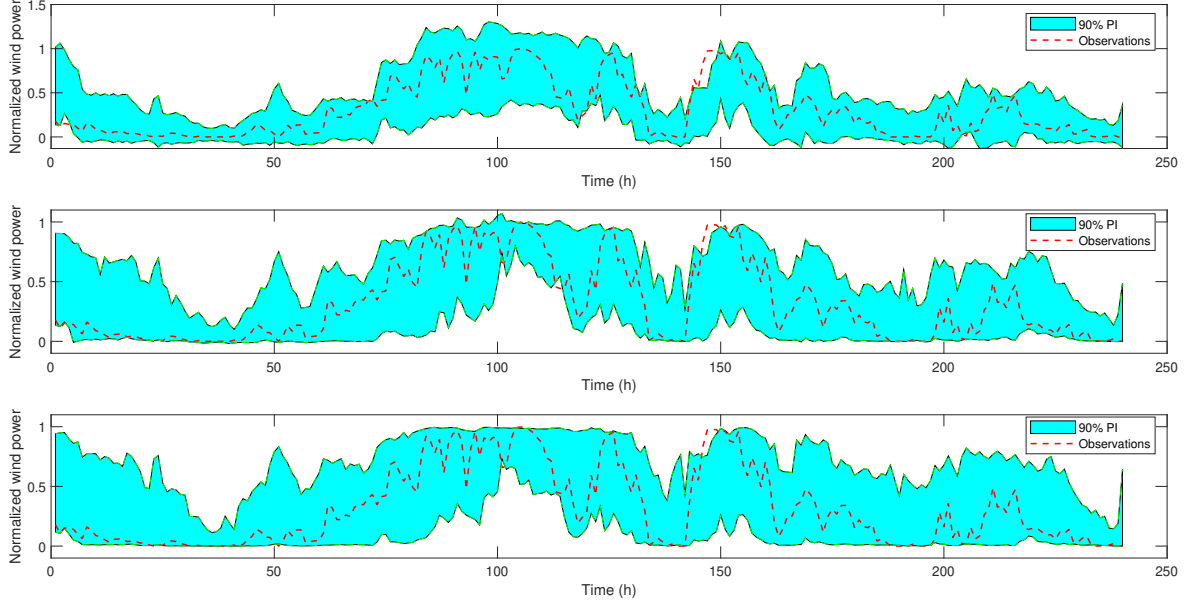
Fig. 9: 90% PI of the proposed model of 10 days at wind farm 1, top: NN-G, middle: proposed, bottom: NN-L.

TABLE IV: CRPS for both France wind farm and NREL dataset (percentage of nominal capacity).

	Climatology	NN-G	NN-L	QRGBM	KDE	MDN	Proposed model
France wind farm	13.40	1.85	1.82	1.92	3.17	2.06	1.83
NREL	21.96	0.25	0.25	0.34	2.58	0.46	0.28

TABLE V: ES for Case 3 and Case 4 (percentage of nominal capacity).

	MuPEn	NN-G	NN-L	Proposed model
Case 3	33.73	9.32	9.20	9.20
Case 4	51.95	2.68	2.64	2.44

TABLE VI: VS in Case 3 and Case 4.

	MuPEn	NN-G	NN-L	Proposed model
Case 3	0.3842	0.2711	0.2377	0.2424
Case 4	0.6303	0.0634	0.0524	0.0446

formats of the proposed model are more flexible than specific families of distributions because the proposed model does not rely on any distributional assumptions. In addition, the proposed model has 1.7 million trainable parameters, which are comparable to those of NN-G and NN-L, i.e., 1.6 million trainable parameters. This means that the proposed model can flexibly model different wind power distribution characteristics on condition of predicted wind speeds, with increased but affordable complexity.

2) Reliability and Sharpness: The reliability diagram and PI width for wind farm 1 are illustrated in Fig. 7 and Fig. 8. It turns out that QRGBM and the proposed model achieve the best performance in reliability, which are close to the ideal case. Strictly speaking, it is unfair to compare a bunch of independently trained QR models with a single model that derives the whole distribution, as the computational cost of QR for a single quantile is much larger. Nevertheless, the proposed model still achieves comparable reliability, which confirms its performance. By contrast, the reliability diagrams of NN-G, NN-L, MDN, and KDE deviate from the ideal to a certain degree. The deviation of NN-G and NN-L cannot be totally mitigated, since the families of distribution they define mismatch the real underlying distribution. Results suggest that the superiority of the proposed model goes beyond the distribution-free property compared to the QR and KDE-based methods, by offering an efficient and continuous conditional modeling approach.

Fig. 8 demonstrates that the proposed model provides the shortest PI in all nominal levels. However, the performance of NN-G in width of PI is comparable to that of the proposed model, whereas the PI width of NN-L is much wider. For illustration, we present 90% PI of the NN-G, proposed model, and NN-L in 10 days in the top, middle, and bottom subplots of Fig. 9. As shown, the PI of NN-G violate the bounds of wind power to a large extent, revealing probability leakage issue, while PIs of the proposed model and NN-L are more realistic. Besides, it is demonstrated that PIs of NN-L are sometimes unnecessarily wide. For example, between 200-

h and 250-h, the upper bound of NN-L is larger than that of NN-G and the proposed model. Indeed, both the NN-L and the proposed model can be considered as models derived from the NN-G by applying transforms. Indeed, the logit-normal transform in the NN-L applies to the whole domain indifferently, whereas the spline transform of the proposed model is piece-wise. This explains the sacrifice of NN-L in PI width, which is a side-effect when forcing the variable into the boundary.

B. Case 2

We present the CRPS of Case 2 in Table IV. As with Case 1, all models are superior to climatology. The performance of NN-G, NN-L, QRGBM and the proposed model are demonstrated to be comparable. The gap of performance between the KDE and others is enlarged compared to Case 1, because of higher dimension of input features which raises issues for k-nearest neighbors. Comparing results of KDE, QRGBM, MDN, and the proposed model with results of NN-G and NN-L, we can infer that the assumptions of Gaussian and logit-normal distribution are fairly adequate in very-short term PWPF. This may be due to the fact that the structure of temporal interdependence over a short period of time is simpler than the interdependence spanning several hours.

C. Case 3 and Case 4

The ES and VS are presented in Table V and Table VI. All of NN-G, NN-L, and the proposed model outperform MuPEn, since the MuPEn draws samples from the empirical unconditional distribution whereas other models draws samples from the estimated conditional distribution. Except for the MuPEn, the ES and VS in Case 3 are larger than those in Case 4, which indicates larger uncertainty in Case 3. This is is caused by the fact that wind power generation uncertainty increases as forecasting horizon increase. In both cases, NN-L and the proposed model exceed NN-G, which suggests the limited capability of the Gaussian assumption in complex and high dimensional cases. Besides, the performance of NN-L and the proposed model are comparable in Case 3, but they differ in Case 4, which suggests that spatial interdependence is more complex.

D. Distribution-free vs Distributional Assumption

In the case study, QRGBM, KDE, and the proposed model are distribution-free, whereas NN-G and NN-L rely on assumptions about specific distributions. Compared to NN-G and NN-L, the proposed model has increased but affordable complexity due to its spline operation. Meanwhile, the increased complexity enables the proposed model to adapt to different wind power distribution characteristics at different predicted wind speeds. Compared to QRGBM and KDE, the proposed model is superior in efficiently modeling whole conditional PDFs. In addition, case studies show that distribution-free methods are not overwhelmingly superior to models with distribution assumptions. Concretely, NN-G and NN-L rival QRGBM and KDE in several cases. And in Case 2, the

performance of NN-L is comparable to that of the proposed model, which means these assumptions are adequate in very-short-term PWPF. But when it comes to scenarios with more uncertainty and more complex interdependence, the proposed approach always achieves a satisfactory performance with an acceptable computational cost. Indeed, it has been reported in [18] that the distribution-free integration-based NF model is comparable to an affine NF model that is equivalent to NN-G. We infer that it is resulted from the difficulty in training the integration-based NF. Intuitively, it will take more effort to find the desired transform in a larger function space. This also reveals the trade-off between efficiency and flexibility in modeling distributions.

E. Discussion on Base Distribution

Theoretically, the base distribution modeled by $\mathcal{G}$ can be set as any distribution. By learning the transforms, one can still obtain the estimation of desired distribution. But it means that one needs to estimate the transforms in a relatively large space, if the base distribution is considerably different from the underlying distribution. For illustration, we consider the wind farm 1 in Case 1 and set the base distribution as a standard Normal distribution $\mathcal{N}(0, 1)$. In theory, this will not make a lot differences in estimated distributions, since the standard Normal can be transformed to any Gaussian by using an affine transform. But compared to the proposed model, this setting implies more complicated task, i.e., the flow model requires to estimate such affine transform besides the non-affine transform. In the experiments, the CRPS under the condition of standard Normal base distribution turns out as 14.9, which is much larger than that of the proposed model, i.e., 9.22. In other words, the estimation of base distribution reveals significance in a practical sense.

F. Training Time

Training time of all models in Case 1 is presented in Table VII, we report the training time of 1000 epochs of NN-based models and 199 independent quantiles of QRGBM. It shows that the training time of the proposed model is comparable to that of commonly used NN-G, which is affordable. In general, the training time of the proposed model is governed by the number of transforms and the number of hidden units. With more transforms and hidden units, the training time will increase. However, it still costs time to generate scenarios for high-dimensional multivariate forecasting.

VI. Conclusions

The approach for probabilistic wind power forecasting described in this paper, based on conditional spline normalizing flow, offers a number of advantages with respect to the existing. It directly estimates the conditional probability density and does not require any assumption on the distributions involved. In addition, it is applicable to both univariate PWPF and multivariate PWPF, with high efficiency in terms of both modeling and computing. Our case-study applications based on open datasets confirmed the interest of the approach and its wide applicability for wind power applications.

TABLE VII: Training time of all models in Case 1 (seconds).

Models	NN-G	NN-L	QRGBM	KDE	MDN	Proposed
Time	56	56	44	14	63	78

TABLE VIII: CRPS under different steps of transforms (percentage of nominal capacity).

Number of Transforms	1	2	3	4	5
CRPS	9.93	9.51	9.23	9.25	9.22

TABLE IX: CRPS under different sizes of hidden units (percentage of nominal capacity).

Number of Units	64	256	512
CRPS	9.22	9.08	9.37

TABLE X: CRPS under different number of knots (percentage of nominal capacity).

Knots	5	10	20	50
CRPS	9.25	9.08	9.19	9.20

Parameters are assumed fixed in this paper; therefore it still needs to explore how to estimate the model in an online learning fashion. Besides, the time for scenario generation is costly when dimension increases, so we will find more efficient methods in the future.

APPENDIX

A. Selection on Hyperparameters

To empirically determine the hyperparameters, we conduct a preliminary test to validate the influence of number of transforms, number of units, and number of knots by studying variants of Case 1. Specifically, we take wind farm 1 as an example, and present results of several case settings.

1) Number of Transforms: In this case, we set the number of hidden units in transform as 64, the number of knots as 10, and vary the number of transforms from 1 to 5. The corresponding results are shown in Table VIII. It can be seen that the CRPS is relatively larger when we use only few transforms. Consequently, the model is small, which results in limited capability of fitting ultimate transform and shape parameter function of base distribution. After reaching at 3 transforms, the gain of increasing transforms is relatively low, which suggest the capability is enough. Besides, increasing transforms means increasing layers of deep neural network, whose training procedure might become difficult when the model is considerably deep.

2) Number of Hidden Units: Here we fix the number of transforms as 5, the number of knots as 10, and adjust the number of hidden units as 64, 256, and 512. Results are presented in Table IX. It shows that the fitting capability of NN in each transform is influenced by the number of hidden units. The capability is limited when the number of hidden units is few. But it might overfit the data if the number of hidden units is considerable.

3) Number of Knots: In this case, we fix the number of layers as 5 and the number of hidden units as 256, and look into the influence of knots by varying the number. We set it as 5, 10, 20, and 50 respectively, whose results are shown in Table X. As we increase the number of knots, the CRPS first decreases and then increases.

REFERENCES

[1] C. Sweeney, R. J. Bessa, J. Browell, and P. Pinson, "The future of forecasting for renewable energy," *Wiley Interdisciplinary Reviews: Energy and Environment*, vol. 9, no. 2, p. e365, 2020.

[2] P. Pinson, H. Madsen, H. A. Nielsen, G. Papaefthymiou, and B. Klöckl, "From probabilistic forecasts to statistical scenarios of short-term wind power production," *Wind Energy: An International Journal for Progress and Applications in Wind Power Conversion Technology*, vol. 12, no. 1, pp. 51–62, 2009.

[3] J. M. Morales, A. J. Conejo, H. Madsen, P. Pinson, and M. Zugno, *Integrating renewables in electricity markets: operational problems.* Springer Science & Business Media, 2013, vol. 205.

[4] M. Lange, "On the uncertainty of wind power predictions—analysis of the forecast accuracy and statistical distribution of errors," *J. Sol. Energy Eng.*, vol. 127, no. 2, pp. 177–184, 2005.

[5] P. Pinson and G. Kariniotakis, "Conditional prediction intervals of wind power generation," *IEEE Transactions on Power Systems*, vol. 25, no. 4, pp. 1845–1856, 2010.

[6] J. B. Bremnes, "A comparison of a few statistical models for making quantile wind power forecasts," *Wind Energy: An International Journal for Progress and Applications in Wind Power Conversion Technology*, vol. 9, no. 1-2, pp. 3–11, 2006.

[7] J. Tastu, P. Pinson, and H. Madsen, "Space-time trajectories of wind power generation: Parametrized precision matrices under a gaussian copula approach," in *Modeling and stochastic learning for forecasting in high dimensions.* Springer, 2015, pp. 267–296.

[8] C. Wan, J. Lin, J. Wang, Y. Song, and Z. Y. Dong, "Direct quantile regression for nonparametric probabilistic forecasting of wind power generation," *IEEE Transactions on Power Systems*, vol. 32, no. 4, pp. 2767–2778, 2016.

[9] M. Landry, T. P. Erlinger, D. Patschke, and C. Varrichio, "Probabilistic gradient boosting machines for gefcom2014 wind forecasting," *International Journal of Forecasting*, vol. 32, no. 3, pp. 1061 – 1066, 2016.

[10] C. Zhao, C. Wan, and Y. Song, "An adaptive bilevel programming model for nonparametric prediction intervals of wind power generation," *IEEE Transactions on Power Systems*, vol. 35, no. 1, pp. 424–439, 2019.

[11] Y. Zhang, H. Wen, Q. Wu, and Q. Ai, "Optimal adaptive prediction intervals for electricity load forecasting in distribution systems via reinforcement learning," 2022.

[12] Y. Zhang, J. Wang, and X. Wang, "Review on probabilistic forecasting of wind power generation," *Renewable and Sustainable Energy Reviews*, vol. 32, pp. 255–270, 2014.

[13] Y. Zhang and J. Wang, "K-nearest neighbors and a kernel density estimator for gefcom2014 probabilistic wind power forecasting," *International Journal of forecasting*, vol. 32, no. 3, pp. 1074–1080, 2016.

[14] M. Afrasiabi, M. Mohammadi, M. Rastegar, and S. Afrasiabi, "Advanced deep learning approach for probabilistic wind speed forecasting," *IEEE Transactions on Industrial Informatics*, vol. 17, no. 1, pp. 720–727, 2020.

[15] O. Makansi, E. Ilg, O. Cicek, and T. Brox, "Overcoming limitations of mixture density networks: A sampling and fitting framework for multi-modal future prediction," in *Proceedings of the IEEE/CVF Conference on Computer Vision and Pattern Recognition*, 2019, pp. 7144–7153.

[16] Y. Chen, Y. Wang, D. Kirschen, and B. Zhang, "Model-free renewable scenario generation using generative adversarial networks," *IEEE Transactions on Power Systems*, vol. 33, no. 3, pp. 3265–3275, 2018.

[17] C. Chu, K. Minami, and K. Fukumizu, "Smoothness and stability in gans," in *Proceedings of the 8th International Conference on Learning Representations*, 2019.

[18] J. Dumas, A. Wehenkel, D. Lanaspeze, B. Cornélusse, and A. Sutera, "A deep generative model for probabilistic energy forecasting in power systems: normalizing flows," *Applied Energy*, 2021, in press, available online.

[19] P. Pinson, "Very-short-term probabilistic forecasting of wind power with generalized logit–normal distributions," *Journal of the Royal Statistical Society: Series C (Applied Statistics)*, vol. 61, no. 4, pp. 555–576, 2012.

[20] H. Wen, J. Ma, J. Gu, L. Yuan, and Z. Jin, "Sparse variational gaussian process based day-ahead probabilistic wind power forecasting," *IEEE Transactions on Sustainable Energy*, 2022.

[21] E. M. Stein and R. Shakarchi, *Princeton lectures in analysis*. Princeton University Press, 2003.

[22] D. Rezende and S. Mohamed, "Variational inference with normalizing flows," in *Proceedings of the 32th International conference on machine learning*, 2015, pp. 1530–1538.

[23] G. Papamakarios, E. Nalisnick, D. J. Rezende, S. Mohamed, and B. Lakshminarayanan, "Normalizing flows for probabilistic modeling and inference," *Journal of Machine Learning Research*, vol. 22, no. 57, pp. 1–64, 2021.

[24] G. Papamakarios, T. Pavlakou, and I. Murray, "Masked autoregressive flow for density estimation," in *Proceedings of the 31st International Conference on Neural Information Processing Systems*, 2017, pp. 2335–2344.

[25] C. Durkan, A. Bekasov, I. Murray, and G. Papamakarios, "Neural spline flows," *Proceedings of the 33th International Conference on Neural Information Processing Systems*, vol. 32, pp. 7511–7522, 2019.

[26] L. Cavalcante, R. J. Bessa, M. Reis, and J. Browell, "Lasso vector autoregression structures for very short-term wind power forecasting," *Wind Energy*, vol. 20, no. 4, pp. 657–675, 2017.

[27] C. Winkler, D. Worrall, E. Hoogeboom, and M. Welling, "Learning likelihoods with conditional normalizing flows," *arXiv preprint arXiv:1912.00042*, 2019.

[28] A. Khosravi, S. Nahavandi, S. Member, D. Creighton, A. F. Atiya, and S. Member, "Comprehensive Review of Neural Network-Based Prediction Intervals and New Advances," *IEEE Transactions on Neural Networks*, vol. 22, no. 9, pp. 1341–1356, 2011.

[29] P. Kou, F. Gao, and X. Guan, "Sparse online warped gaussian process for wind power probabilistic forecasting," *Applied energy*, vol. 108, pp. 410–428, 2013.

[30] C.-W. Huang, D. Krueger, A. Lacoste, and A. Courville, "Neural autoregressive flows," in *Proceedings of the 35th International Conference on Machine Learning*, J. Dy and A. Krause, Eds., vol. 80, 10–15 Jul 2018, pp. 2078–2087.

[31] M. Germain, K. Gregor, I. Murray, and H. Larochelle, "Made: Masked autoencoder for distribution estimation," in *Proceedings of the 32nd International Conference on Machine Learning*, 2015, pp. 881–889.

[32] T. Hastie, R. Tibshirani, J. H. Friedman, and J. H. Friedman, *The elements of statistical learning: data mining, inference, and prediction*. Springer, 2009, vol. 2.

[33] J. W. Messner, P. Pinson, J. Browell, M. B. Bjerregård, and I. Schicker, "Evaluation of wind power forecasts—an up-to-date view," *Wind Energy*, vol. 23, no. 6, pp. 1461–1481, 2020.

[34] P. Pinson and R. Girard, "Evaluating the quality of scenarios of short-term wind power generation," *Applied Energy*, vol. 96, pp. 12–20, 2012.

[35] M. Scheuerer and T. M. Hamill, "Variogram-based proper scoring rules for probabilistic forecasts of multivariate quantities," *Monthly Weather Review*, vol. 143, no. 4, pp. 1321–1334, 2015.

[36] D. van der Meer, "A benchmark for multivariate probabilistic solar irradiance forecasts," *Solar Energy*, vol. 225, pp. 286–296, 2021.

[37] D. P. Kingma and J. Ba, "Adam: A method for stochastic optimization," *CoRR*, vol. abs/1412.6980, 2014.